Supplementary Information

A Fingerprint of Metal-oxide Powders: Energy-resolved Distribution of Electron Traps

Akio Nitta, Mai Takase, Mai Takashima, Naoya Murakami and Bunsho Ohtani

Reversed double-beam photoacoustic spectroscopy (RDB-PAS)

The original setups and procedures for conventional photoacoustic spectroscopy (PAS) and double-beam photoacoustic spectroscopy (DB-PAS) have been reported in detail [(ref. 6) N. Murakami, O.-O. Prieto-Mahaney, R. Abe, T. Torimoto and B. Ohtani, *J. Phys. Chem. C*, 2007, **111**, 11927-11935.]. In PAS and DB-PAS, a modulated (chopped) light beam creating a PA signal is wavelength-scanned to obtain a PA spectrum of samples, and continuous monochromatic or polychromatic continuous light, which does not have any effect on the PA signal, is overlapped in DB-PAS to drive photochemical reactions by the continuous light irradiation with in-situ PA spectrum acquisition. In reversed double-beam photoacoustic spectroscopy (RDB-PAS), modulated and continuous light beams in DB-PAS are exchanged; continuous wavelength-scanning light is illuminated to excite VB electrons to electron traps (ETs), and modulated monochromatic light is simultaneously irradiated to a powder sample to detect photoabsorption of electron-filled ETs, i.e., action spectrum for photoinduced trap filling is recorded (Table S1).

The setup for RDB-PAS was as follows (**Fig. S1**). A home-made aluminum PAS cell with a quartz window and a microphone (Knowles Electronics SP0103NC3-3 electret condenser microphone) was used [(ref. 6) N. Murakami, O.-O. Prieto-Mahaney, R. Abe, T. Torimoto and B. Ohtani, *J. Phys. Chem. C*, 2007, **111**, 11927-11935.]. A powder sample (15–110 mg) was set in a sample holder in the cell, and ambient-temperature argon flow saturated with methanol vapor was made to flow through the cell for at least 30 min and then the cell was sealed off. The purpose of methanol saturation in the measurement is to capture those positive holes irreversibly and thereby to avoid disappearance of once-trapped electrons through the reaction with positive holes. A monochromatic light beam from a xenon lamp (Spectral Products ASB-XE-175 xenon light source) equipped with a grating monochromator (Spectral Products CM110 1/8m grating monochromator) and an LED beam (Luxeon LXHL-ND98 625-nm light-emitting diode) voltage-

Table S1 Comparison of photoacoustic spectroscopy (PAS), double-beam photoacoustic spectroscopy (DB-PAS) and reversed double-beam photoacoustic spectroscopy (RDB-PAS).

mode	modulated light	continuous light	spectrum
PAS	wavelength scanning	–	photoabsorption
DB-PAS	wavelength scanning	no scanning	in-situ photoabsorption
RDB-PAS	no scanning	wavelength scanning	trap-filling action

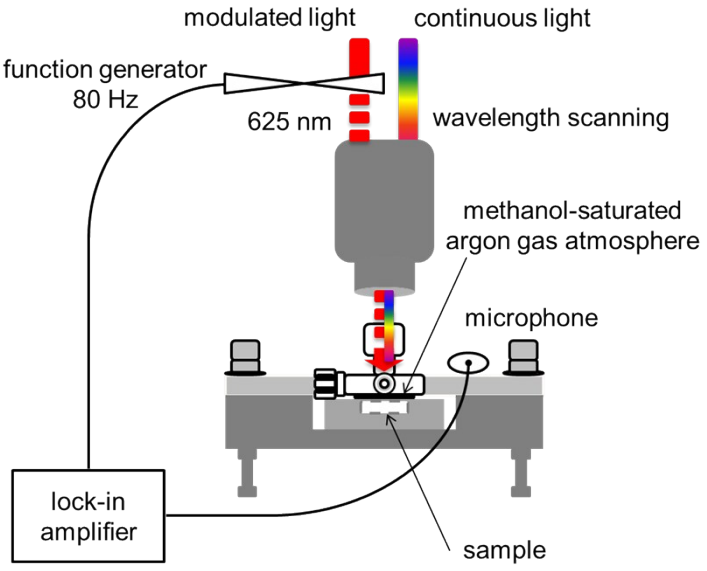

Figure S1 Schematic representation of the setup for RDB-PAS.

modulated (80 Hz) by a function generator (NF Corporation DF1906 digital function generator) were mixed by a UV quartz combiner light guide (Moritex MWS5-1000S-UV3) and irradiated from the upper side of the sample cell. The PA signal was acquired in lock-in mode (NF Corporation LI5630 digital lock-in amplifier) and averaged at each wavelength of continuous light during scanning from 650 nm to 350 nm with a 5-nm step. In the conventional PAS analysis, PA signal intensity is calibrated with a blank using graphite as a black body to compensate for wavelength-dependent light intensity, but no such calibration is made in RDB-PAS since the signal intensity, corresponding to the total accumulated trapped-electron density, is independent of continuous-light intensity and modulated-light intensity is constant throughout an acquisition. The thus-obtained RDB-PAS spectrum, a plot of total accumulated electron-trap density as a function of photon energy (E/eV = 1240/(wavelength/nm)) of continuous light (**Fig. S2(a)**), was differentiated from the smaller-energy side to obtain ERDT as a function of energy as reference to the VBT (valence-band top) (**Fig. S2(b)**). The absolute density of ETs was calibrated by comparison with total density of ETs observed by the photochemical method [(ref. 5) S. Ikeda, N. Sugiyama, S.-y. Murakami, H. Kominami, Y. Kera, H. Noguchi, K. Uosaki, T. Torimoto and B. Ohtani, *Phys. Chem. Chem. Phys.*, 2003, **5**, 778-783.] for samples of TIO-2 and CR-EL shown in **Fig. 2**.

In this study, it is assumed that photoabsorption coefficient of electron-filled ETs is constant not depending on their energy (position) without any supporting results. However, similarity in shape of ERDT patterns obtained using RDB-PAS and the photochemical method in **Fig. 2** for two kinds of titania samples suggests the reasonableness of the assumption, since results the photochemical method does not depends on the photoabsorption coefficient of electron-filled ETs.

Conventional PA spectra using a single chopped light beam were recorded in the setup of RDB-PAS; the wavelength-scanned light from a xenon lamp/monochromator was attenuated and chopped (80 Hz), and the PA signal was detected and averaged. The spectra were calibrated with the spectrum taken for graphite to compensate for wavelength-dependent light intensity. The bandgap of a sample was simply determined by extrapolating the linear part of a rise in the shorter wavelength region (**Fig. S2(c)**); a Tauc plot, which is frequently used for determination of the bandgap, was not used due to the ambiguity of decision of direct/indirect transitions (D. E. Scaife, *Solar Energy*, 1980, **25**, 41-54.; B. Ohtani, *Phys. Chem. Chem. Phys.*, 2014, **16**, 1788-1797.).

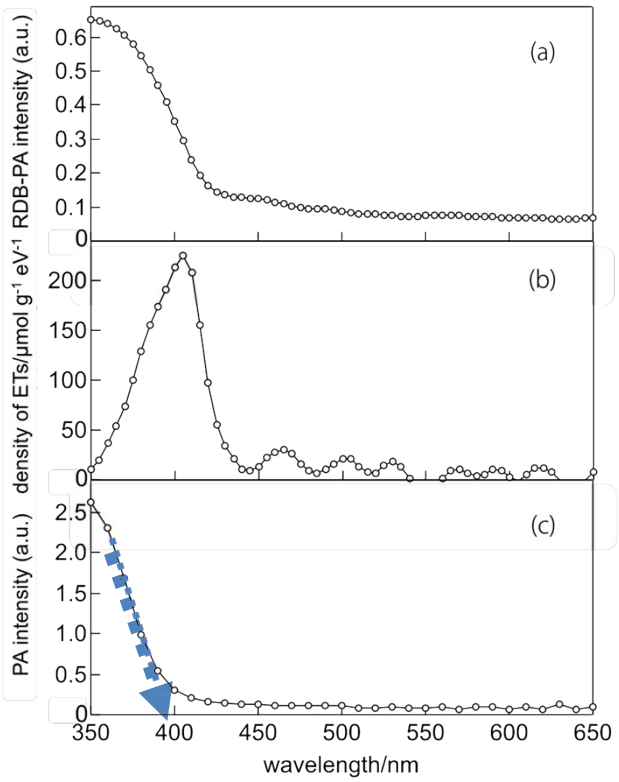

Figure S2 Examples of data acquisition and processing for a representative sample (Catalysis Society of Japan TIO-1). (top) RDB-PA spectrum, (middle) ERDT pattern in the unit of μmol g^{-1} as a function of wavelength of the continuous light by differentiation of RDB-PA spectrum and (bottom) conventional PA spectrum for determination of the band-gap energy. The ERDT pattern (middle) is replotted as a function of energy from VBT as shown in **Fig. 1**.

Correlation between total electron-trap density and specific surface area

Figure S3 shows the correlation. An almost linear relation that did not depend on the kind of crystallites, anatase, rutile and their mixture was observed. The y-intersect, ca. 14 μmol g^{-1} (= 2.1×10^{-18} cm^{-3} assuming a density of 4 g cm^{-3}, one or two orders of magnitude higher than the electron-trap density reported for thin films of anatase [(ref. 2) T. Miyagi, T. Ogawa, M. Kamei, Y. Wada, T, MitsuhashiI, A. Yamazaki, E, Ohta and T. Sato, *Jpn. J. Appl. Phys.* 2001, **40**, L404–L406.]), might correspond to ETs in bulk. The slope of the linear plot, ca. 1.6×10^{-6} mol m^{-2} = 1.0 nm^{-2}, might reflect the surface density of ETs.

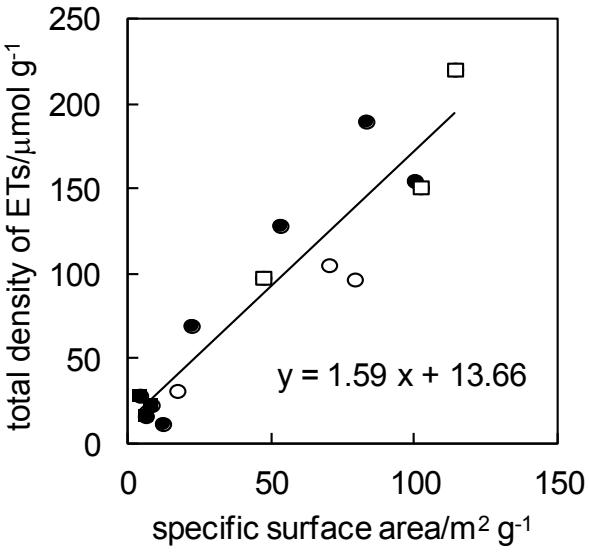

Figure S3 Correlation between total density of ETs and specific surface area of representative titania samples. Open circles and squares denote anatase and retile samples, respectively, and closed circles and squares denote anatase-rich and rutile-rich samples, respectively.

ERDT/CBB patterns of metal-oxide powders other than titania

Since metal oxides are, in general, n-type semiconductors having bandgaps and donor levels below the CBB, it is no surprise that metal oxides other than titania may exhibit ERDT/CBB patterns, as shown in **Fig. S4**. As expected, the CBBs were different, reflecting different electronic structures of their bulk. The ERDT patterns were also different depending on the kind of metal oxide, but ERDT patterns of the same metal-oxide samples may also be different as has been seen for titania samples.

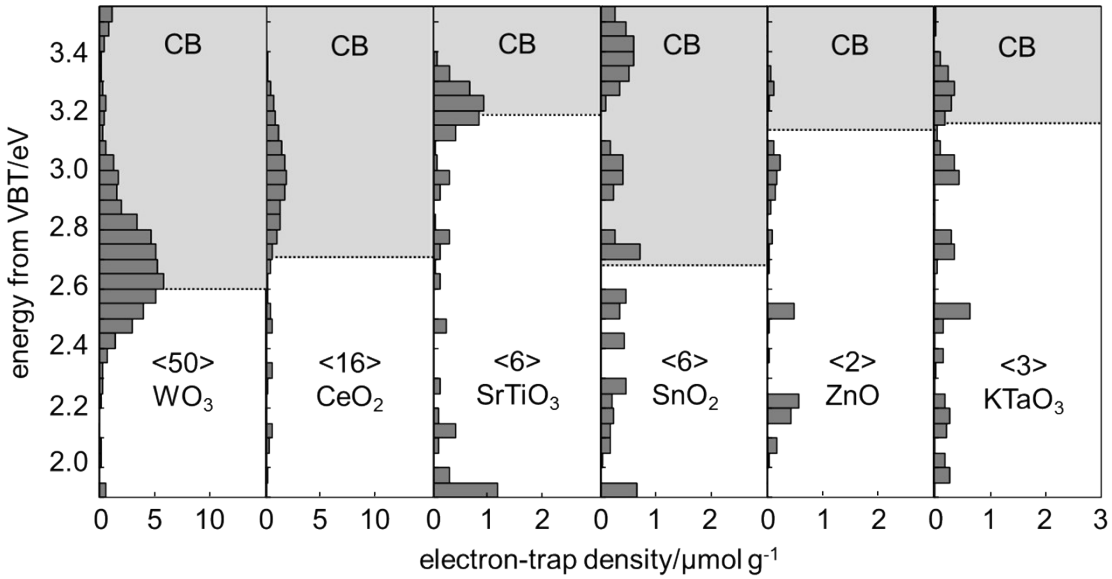

Figure S4 Representative ERDT patterns with CBB position for commercially available tungsten(VI) oxide (Kojundo Chemical Laboratory), cerium(IV) oxide (Kojundo Chemical Laboratory), strontium titanate (Sigma-Aldrich), tin(IV) oxide (Wako Pure Chemical Industries), zinc oxide (Wako Pure Chemical Industries) and potassium tantalate (Kojundo Chemical Laboratory). Figures in <> show total electron-trap density in the unit of μmol g^{-1}.

Applicability of the degree of coincidence of ERDT/CBB patterns for identification of samples of metal oxides other than titania is now being examined and the results will be reported in the future.

Ranking of high degree of coincidence ζ

The top seven ranked high-ζ (> 0.6) pairs of commercially available or non-profitably provided titania samples are shown in Table S2.

Table S2 Top seven ranked high-ζ (> 0.6) pairs of commercially available or non-profitably provided titania samples

rank	pair		ζ	ζ(a): ERDT pattern shape	ζ(b): total density of ETs	ζ(c): CBB	ζ_{pc}[a]
1	TIO-4[b]	Wako[c]	0.788	0.863	0.941	0.970	0.901
2	TIO-4[b]	P25	0.760	0.810	0.939	0.999	0.884
3	TIO-8[b]	ST-01	0.751	0.851	0.885	0.996	0.839
4	P25	Wako	0.723	0.844	0.884	0.969	0.848
5	TIO-6[b]	MT-150A	0.705	0.856	0.828	0.995	0.793
6	TIO-13[b]	FP-6	0.684	0.847	0.827	0.976	0.748
7	TIO-11[b]	FP-6	0.615	0.620	0.998	0.994	0.697

[a]Average of ζ_{pc} for the three photocatalytic reactions. [b]Reference titania provided by Catalysis Society of Japan. [c]Code 207-11121 (208-18231), Wako Pure Chemical Industries Ltd.

Photocatalytic activity test

Three representative photocatalytic reactions, (a) hydrogen liberation from deaerated aqueous methanol, (b) carbon-dioxide liberation from aqueous acetic acid under aerobic conditions and (c) oxygen evolution from aqueous silver fluoride, were used. A brief explanation of the experimental procedures is as follows [(ref. 12) B. Ohtani, O.-O. Prieto-Mahaney, F. Amano, N. Murakami and R. Abe, *J. Adv. Oxidat. Tech.* 2010, **13**, 247–261.]. A standard amount of the powder photocatalyst (50 mg) was suspended in an aqueous solution (5.0 mL) in a borosilicate glass tube (transparent for wavelength > 290 nm, 18 mm in inner diameter and 180 mm in length) containing methanol (50 vol%) and chloroplatinic acid ($H_2PtCl_6 \cdot 6H_2O$; corresponding to 2-wt% platinum (Pt) loading), acetic acid (5.0vol%), and silver fluoride (50 mmol L^{-1}) in reactions (a), (b), and (c), respectively. Air was purged off from the systems by passing argon through the suspensions for at least 15 min, and the sample tubes were tightly sealed using a double-capped rubber septum and a sheet of Parafilm to prevent leakage of gas and/or contamination. The samples were irradiated by a 400-W high-pressure mercury arc (Eiko-sha) at 298 K under vigorous magnetic stirring (1000 rpm). Reactions (a), (b) and (c) were monitored by analyzing liberation of hydrogen (H_2), carbon dioxide (CO_2) and oxygen (O_2), respectively, by gas chromatography (Shimadzu GC-8A gas chromatograph equipped with a TCD and columns of molecular sieve 5A for H_2 and O_2 and Porapak Q for CO_2). Activities (*A*s) were calculated as the rate of product formation.